JACS
JOURNAL OF THE AMERICAN CHEMICAL SOCIETY
Article
pubs.acs.org/JACS

Using Hollow Carbon Nanospheres as a Light-Induced Free Radical Generator To Overcome Chemotherapy Resistance

Liming Wang,[†,∥] Qiang Sun,[‡,∥] Xin Wang,[†] Tao Wen,[†] Jun-Jie Yin,[§] Pengyang Wang,[†] Ru Bai,[†] Xiang-Qian Zhang,[‡] Lu-Hua Zhang,[‡] An-Hui Lu,*[,‡] and Chunying Chen*[,†]

[†]CAS Key Laboratory for Biomedical Effects of Nanomaterials and Nanosafety, National Center for Nanoscience and Technology of China and Institute of High Energy Physics, Chinese Academy of Sciences, Beijing China

[‡]State Key Laboratory of Fine Chemicals, School of Chemical Engineering, Dalian University of Technology, Dalian 116024, China

[§]Division of Analytical Chemistry, Office of Regulatory Science, Center for Food Safety and Applied Nutrition, U.S. Food and Drug Administration, College Park, Maryland 20740, United States

Supporting Information

ABSTRACT: Under evolutionary pressure from chemotherapy, cancer cells develop resistance characteristics such as a low redox state, which eventually leads to treatment failures. An attractive option for combatting resistance is producing a high concentration of produced free radicals *in situ*. Here, we report the production and use of dispersible hollow carbon nanospheres (HCSs) as a novel platform for delivering the drug doxorubicine (DOX) and generating additional cellular reactive oxygen species using near-infrared laser irradiation. These irradiated HCSs catalyzed sufficiently persistent free radicals to produce a large number of heat shock factor-1 protein homotrimers, thereby suppressing the activation and function of resistance-related genes. Laser irradiation also promoted the release of DOX from lysosomal DOX@HCSs into the cytoplasm so that it could enter cell nuclei. As a result, DOX@HCSs reduced the resistance of human breast cancer cells (MCF-7/ADR) to DOX through the synergy among photothermal effects, increased generation of free radicals, and chemotherapy with the aid of laser irradiation. HCSs can provide a unique and versatile platform for combatting chemotherapy-resistant cancer cells. These findings provide new clinical strategies and insights for the treatment of resistant cancers.

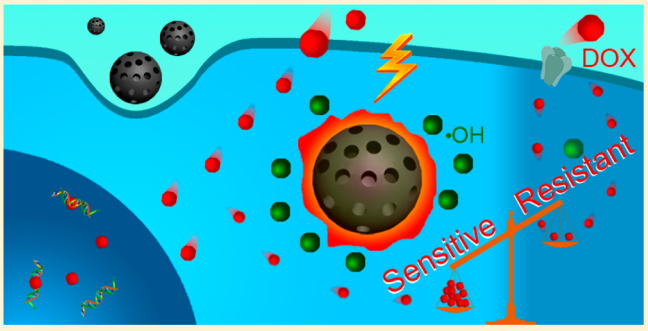

INTRODUCTION

The development of resistance to chemotherapy and subsequent treatment failures are serious obstacles in cancer therapy.[1] Once resistance develops, higher doses of available drugs may be ineffective, resulting in strong toxic side effects.[2,3] Oncologists must switch their patients to alternative treatment regimens or, if alternatives are either unavailable or unacceptable, offer palliative care. Doxorubicine (DOX) is a widely accepted drug used to suppress the growth and survival of human breast cancers; however, under selection pressure, cancer cells frequently develop DOX resistance by overexpressing the multidrug resistance gene (MDR-1) or by encoding an efflux pump protein, P-glycoprotein (Pgp) that exports the drug and prevents intracellular levels of the DOX from reaching therapeutic levels.[4] Other mechanisms of resistance are mutations to the pro-apoptosis protein, p53, which allows such cells to escape apoptosis,[5,6] and adaptations which allow cancer cells to endure the oxidative stress induced by toxic drugs and maintain redox homeostasis, a low redox state.[7−9] To improve cancer therapy outcomes, strategies must be developed to correct or combat these adaptations, particularly oxidation resistance.[8]

Countermeasures to inhibit these forms of resistance have included attempting to restore normal endocytosis (to increase the uptake of anticancer agents),[10−12] suppressing the expression of exporter proteins or weakening their functions,[13−16] repressing the expression of antiapoptosis proteins,[17,18] suppressing detoxification abilities, and increasing levels of oxidative stress.[19,20] The design of nanomaterials with the tunable properties[21] offers great promise for combatting resistance. Multifunctional nanocarriers have been shown to successfully deliver and release drugs,[10,22] carry small interfering RNA (siRNA),[15] and increase oxidative stress through extrinsic physical stimuli.[23−26] However, few reports have examined whether nanocarriers can simultaneously overcome the main characteristics of DOX-resistant cancer cells by enabling higher intracellular accumulation of drugs, improving sensitivity to those drugs, and interfering with redox homeostasis. This strategy could reduce or eliminate treatment resistance, and increase the likelihood of long-term treatment success.[17]

Received: November 10, 2014
Published: January 17, 2015

DOI: 10.1021/ja511560b
J. Am. Chem. Soc. 2015, 137, 1947−1955

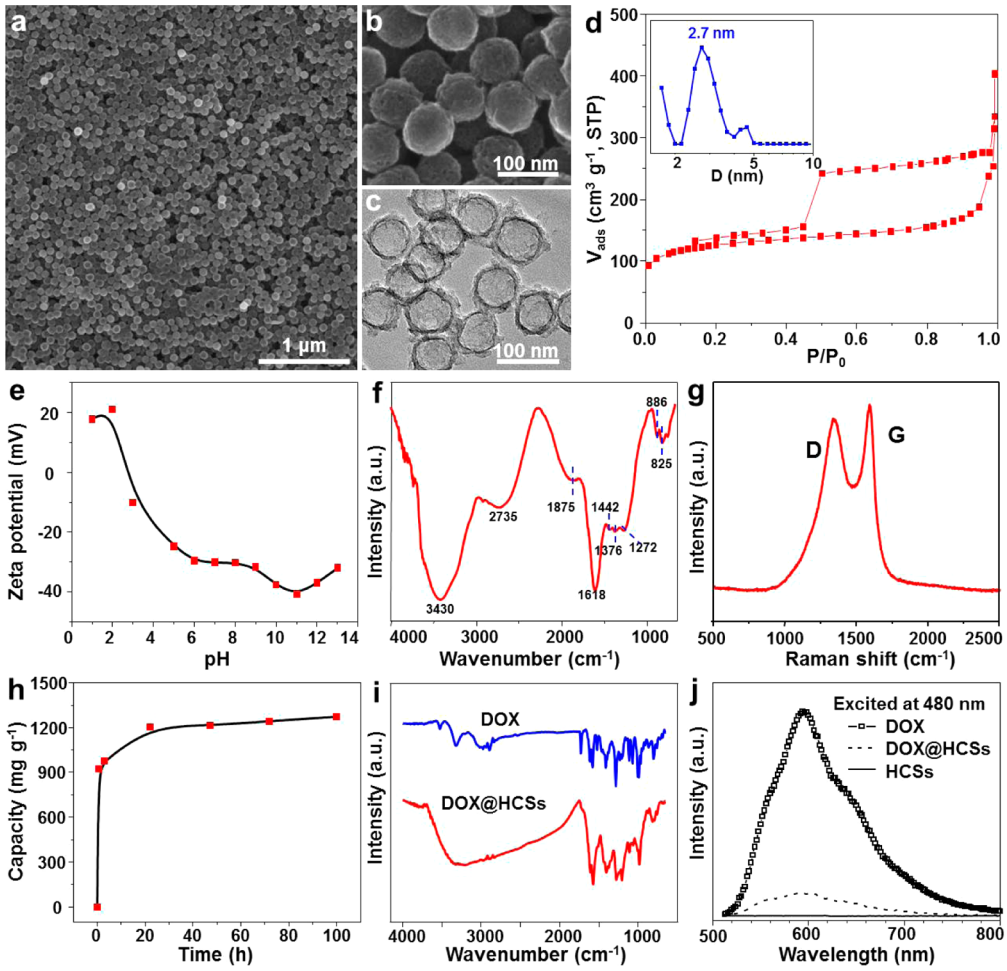

Figure 1. Characterization of hollow carbon nanospheres (HCSs). (a and b) SEM and (c) TEM images, (d) N_2 adsorption−desorption isotherms, (e) zeta potential measurement, (f) FTIR spectrum, (g) Raman spectrum, and (h) DOX loading capacity of HCSs (DOX@HCSs) in water at 30 °C as determined from the absorption spectrum at 480 nm. (i) FTIR spectra of free DOX, and DOX@HCSs. (j) The fluorescence emission spectra of 60 μg mL^{-1} DOX, 110 μg mL^{-1} DOX@HCSs, and 50 μg mL^{-1} HCSs.

Previous studies have established that gold nanorods[22,27] and graphene[28,29] nanomaterials as efficient drug and gene carriers for biomedicine. Carbon nanomaterials have attracted much attention for cancer therapy.[28−31] In particular, porous carbons and hollow carbon nanospheres (HCSs) have higher surface areas and larger pore volumes than gold nanorods.[32−37] As HCSs feature sp^2- and sp^3-bonded carbon atoms and many mesopores on their external and internal surfaces, they have a great capacity to adsorb and load relatively large amounts of drugs.[38−40] Moreover, carbon nanospheres provide more biocompatibility compared with tube- and lamella-like nanomaterials, because the latter are at greater risk of rupturing the membrane structures of cells.[41,42] In addition, these sp^2 and sp^3 carbon nanostructures usually exhibit good catalytic activity[43] and can induce the generation of free radicals in the biological systems.[44−47] This potential to upset redox homeostasis and/or to trigger stress-mediated responses in biological systems[44,48,49] may be essential to overcoming chemotherapy resistance.

Although HCSs have many features which should make them effective carriers for chemotherapeutic agents, there are two obstacles to their use. First, HCSs prepared using conventional methods are usually too large to be effectively internalized by most cancer cells. Second, due to the incidental coalescence and sintering of all carbon nanostructures during high temperature annealing, HCSs are very difficult to disperse in an aqueous solution, making intravenous administration of drugs associated with HCSs and their circulation in the blood almost impossible. Thus, although it is still a great technical challenge, it is highly desirable to produce HCSs having a uniform size below 100 nm that can also be easily dispersed in water. Our synthesis meets these criteria, resulting in solvent-dispersible, discrete, and uniformly sized HCSs suitable for biomedical applications.

Inspired by the important properties of sp^2 and sp^3-carbon, we have designed HCSs with an optimal diameter of ca. 90 nm as a versatile platform for administering treatments to drug-resistant cancers that will not only deliver drugs such as DOX but can increase the intracellular redox state in response to brief laser irradiation. We had measured the time-dependent changes of cellular reactive oxygen species (ROS) after mild hyperthermia stimulus by a laser and observed a persistent correlation of increased oxidative stress status with an increased expression of the HSF-1 gene that combats drug resistance. Our approach demonstrates novel physical properties for HCSs and how their synergistic effects can overcome chemoresistance adaptations in cancer cells. These innovations should improve the efficacy of cancer treatments and improve the durability of patient responses to those treatments.

DOI: 10.1021/ja511560b
J. Am. Chem. Soc. 2015, 137, 1947−1955

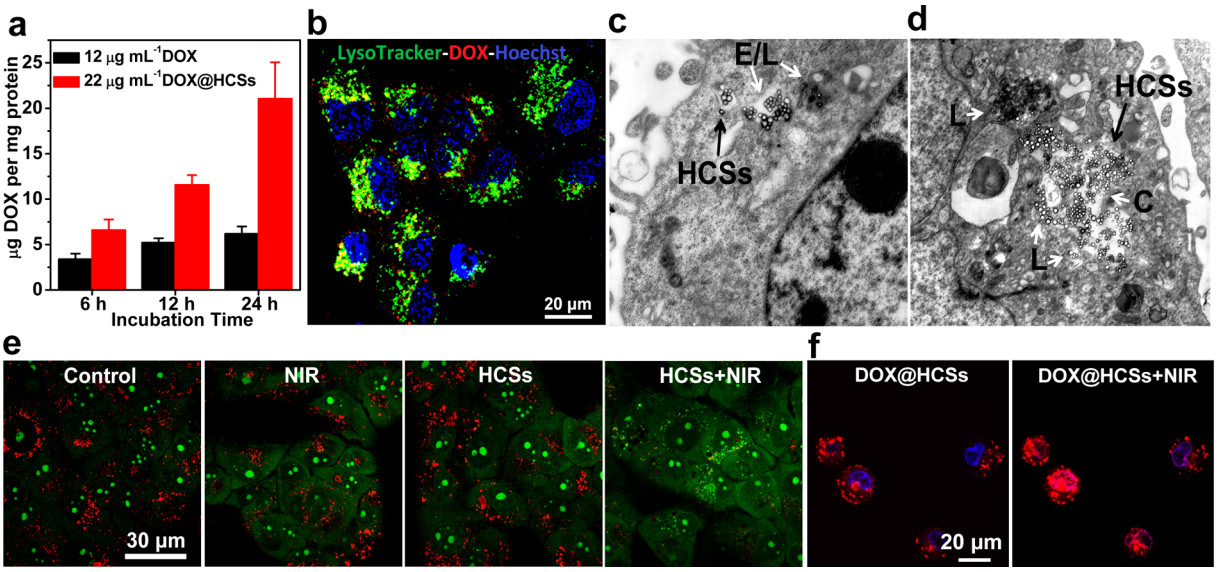

Figure 2. (a) The cellular accumulation of DOX in the formulation of DOX@HCSs. MCF-7/ADR cells are incubated with 12 μg mL^{-1} DOX and 22 μg mL^{-1} DOX@HCSs for 6, 12, and 24 h (LysoTracker, green; DOX, red; Hoechst, blue). (b) Intracellular localization of DOX@HCSs after uptake for 6 h observed by confocal microscope. TEM images of the localization of HCSs (c) before and (d) after NIR irradiation. (e) Changes in the lysosomal membrane permeation induced by the photothermal effects determined by AO staining. E/L indicates endo/lysosomes. (f) Enhanced DOX release from intracellular DOX@HCSs induced by the photothermal effects and DOX entry into the nuclei (DOX, red; Hoechst, blue).

RESULTS AND DISCUSSION

Preparation and Characterization of HCSs and DOX@HCSs. Discrete HCSs were synthesized by confined nanospace pyrolysis using polybenzoxazine polymer nanospheres as the carbon precursor. The scanning electron microscope (SEM) image in Figure 1a shows that these HCSs were spherical, with a uniform diameter of 90 nm; the higher resolution image in Figure 1b shows that they have a rough surface. The transmission electron microscope (TEM) image (Figure 1c) confirmed this spherical morphology and indicated a hollow nanostructure containing a cavity with a diameter of ca. 70 nm and a carbon shell ca. 10 nm in thickness. This unique nanostructure, featuring mesopores, a rough surface, and a hollow cavity, is appropriate for adsorbing and delivering drug molecules or other active substances.

We evaluated the porosity of these nanocarbons using nitrogen adsorption- desorption measurements. As shown in Figure 1d, N_2 adsorption−desorption isotherms of HCSs show a type H_2 hysteresis, characteristic of mesopores. The adsorption isotherm exhibits a slight step at a relative pressure (P/P_0) of 0.14−0.32, corresponding to a pore size of 2.7 nm (inset in Figure 1d). The HCSs had a BET surface area of 434 m^2 g^{-1} and a total pore volume of 0.62 cm^3 g^{-1}. The zeta potential of HCSs was measured in aqueous solutions at different pH values. The surface charge of the sample was shown to switch from positive to negative as the pH increased from 1 to 13 (Figure 1e). In the pH scale ranging from 6 to 13, the zeta potential value was >30 mV or < −30 mV, indicating that these nanoparticles were stably dispersed in an aqueous solution (Supporting Information Figure S1b and Table S1) and in physiological media or buffers containing 10% fetal bovine serum (Supporting Information Table S2). In addition, the negatively charged carbon surface should be able to adsorb positively charged DOX molecules with a zeta potential of 21.6 ± 0.2 mV through electrostatic interaction.

A Fourier transform infrared spectroscopy (FTIR) was used to analyze the functional groups present in the HCSs. Broad peaks at 3430 and 2735 cm^{-1} (Figure 1f) can be attributed to the stretching vibration of O−H and C−H, respectively. The prominent intense contribution at ca. 1618 cm^{-1} can be assigned to the C=O stretching vibration.[28] Together, the peaks at 1875, 1442, 1376, 1272, 886, and 825 cm^{-1} indicated the existence of deformation vibrations of C−H and O−H bands in HCSs.[50,51] These results suggest that the HCSs possess oxygen-containing groups such as hydroxyl, carboxyl, or alkoxy, which were introduced by thermal decomposition of the organic polymer.[50,51] These oxygen-containing groups probably form strong hydrogen bonds with water molecules, thereby increasing the dispersibility of HCSs in water.

The local graphitic structure of the sample was examined using Raman spectroscopy. As shown by Raman spectra (Figure 1g), two most intense features were observed, namely the G peak at ca. 1585 cm^{-1} and a band at ca. 1340 cm^{-1}, historically referred to as the D peak. The G peak arises from doubly degenerate zone center E_{2g} mode, while zone-boundary phonons give rise to the D peak in defect-containing graphite.[52]

By immersing these HCSs in a DOX/DMSO solution, the effective DOX storage capacity was monitored by UV−vis-NIR absorption spectrometry at 480 nm (Supporting Information Figure S2a). The effective capacity of HCSs in DOX loading as a function of reaction time is shown in Figure 1h. The amount of DOX loaded in the HCSs was found to be approximately 54.5%. This high capacity was attributed to the large surface area to pore volume ratio, the formation of cavities, and electrostatic interactions between the positively charged DOX molecules and the negatively charged carbon surface of the HCSs. The graphite plane in HCSs can interact strongly with the DOX aromatic molecule through $\pi-\pi$ stacking, which also contributes to the high loading capacity.[40] As measured by FTIR spectra, DOX@HCSs exhibited characteristic peaks between 750 and 1750 cm^{-1} for DOX (Figure 1i). As shown in Figure 1j, the fluorescence emission spectra of DOX, DOX@HCSs, and pure HCSs. Compared with DOX and DOX@HCSs, adsorption on the carbon surface quenched the

DOI: 10.1021/ja511560b
J. Am. Chem. Soc. 2015, 137, 1947−1955

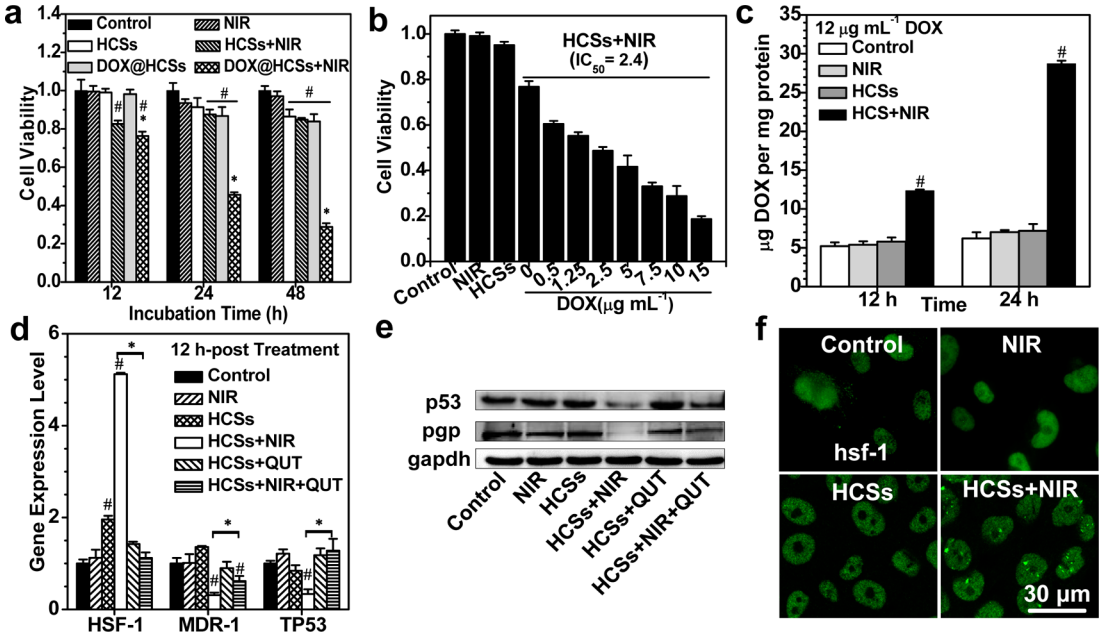

Figure 3. Using laser irradiation and intracellular HCSs to combat DOX resistance. (a) Changes in the viability of MCF-7/ADR cells after treatment with HCSs and DOX@HCSs in the presence and absence of laser irradiation. (b) Changed sensitivity of HCSs-treated MCF-7/ADR cells to DOX at 48 h after laser irradiation. (c) The effects of laser irradiation on the accumulation of DOX in MCF-7/ADR cells. (d and e) The impact of laser irradiation and HSF-1 gene inhibitor (Quercetin, QUT) on gene expression related to DOX-resistance at (d) the mRNA level and (e) the protein level. Asterisk (*) indicates significant differences between the test samples and the control and pound symbol (#) shows significant differences between test samples and the HCSs together with near-infrared (NIR) laser irradiation (HCSs + NIR) ($p < 0.05$). (f) The change in the number of hsf-1 protein homotrimers in the nucleus after laser irradiation.

fluorescence of DOX at an equivalent dosage (60 μg mL^{-1}), also indicative of successful loading of DOX into the HCSs.

Cytotoxicity, Cell Uptake, and Localization of HCSs and DOX@HCSs. To demonstrate that whether the HCSs carrying DOX are able to reduce DOX resistance in cancer cells, we evaluated their effectiveness as follows. We confirmed the resistance to DOX of cultured human breast cancer cells (MCF-7/ADR) by treating samples with different DOX concentrations. The half-inhibitory concentration (IC_{50}) was defined as the concentration at which a drug reduces cell viability by 50%. Based on CCK-8 assay, cell viability results show that MCF-7/ADR cells had a high capacity to tolerate DOX, with an IC_{50} which was approximately 24.6 times higher than that of sensitive human breast cancer cells (MCF-7) after 48 h (Supporting Information Figure S3a,b). HCSs were shown as a biocompatible nanocarrier with MCF-7/ADR cells and normal human breast epithelial cells (MCF-10A) (Supporting Information Figure S3c,f). HCSs induced a low toxicity (less than 10%) to MCF-7/ADR cells below 10 μg mL^{-1}, while DOX-loaded HCSs (DOX@HCSs) caused cytotoxicity in a dose- and time-dependent effect (Supporting Information Figure S3c,d). We then prepared a mild dose consisting of 10 μg mL^{-1} HCSs, 12 μg mL^{-1} DOX, and the equivalent 22 μg mL^{-1} DOX@HCSs for use in the following experiments.

MCF-7/ADR cells tend to accumulate DOX to a less degree compared with sensitive cells due to high expression of the membrane pump protein Pgp responsible for DOX efflux. More specifically, MCF-7/ADR cells are capable of internalizing higher amount of DOX in the form of DOX@HCSs compared with free DOX alone. Results showed that DOX@HCSs were internalized in a time-dependent manner and that DOX accumulation increased by nearly three times after 24 h (Figure 2a). In the DOX@HCSs drug delivery system, HCSs were used as nanocarriers to encapsulate DOX, which increased the amount of internalized DOX by endocytosis and reduced DOX efflux by Pgp proteins. As shown in Figure 2b, the red fluorescence indicated DOX and the green fluorescence indicated the lysosome. The colocalization results show that after 6 h incubation, the DOX@HCSs or the released DOX mainly localized in the lysosomes and seldom in the nuclei (Figure 2b). The TEM results confirmed the localization of HCSs in the endo/lysosomes after 24 h uptake (Figure 2c, and Supporting Information Figure S4a,b).

The temperature at which the cancer cells were exposed to DOX and DOX@HCSs had a noticeable impact on efficacy. Although the MCF-7/ADR cells exhibited higher accumulations, DOX@HCSs at 37 °C did not decrease cell viability to a greater degree compared with free DOX did (Supporting Information Figure S3b,d) due to the low release profile, which is ca. 20% of DOX alone (Supporting Information Figure S2e),and therefore,the HCSs had poor capability to overcome resistance (Supporting Information Figure S3e). However, as shown by DOX release profile in Supporting Information Figure S2e at 43 °C, DOX@HCSs displayed a higher level efficiency of DOX release (ca. 40%), suggesting that photothermal treatment using NIR irradiation may reduce the survival of resistant cells.

Photothermal Effects of HCSs under NIR Laser Irradiation. Uniform and discrete HCSs had strong and wide range of light absorption, from ultraviolet to near-infrared (Supporting Information Figure S2b); thus, HCSs should exhibit excellent heat generation under near-infrared irradiation. When irradiated, HCSs exhibited a power density-dependent photothermal therapy effect (Supporting Information Figures S2c) that correlated with the deaths of cells containing HCSs (Supporting Information Figure S5a,b). On irradiation by a 780

DOI: 10.1021/ja511560b
J. Am. Chem. Soc. 2015, 137, 1947−1955

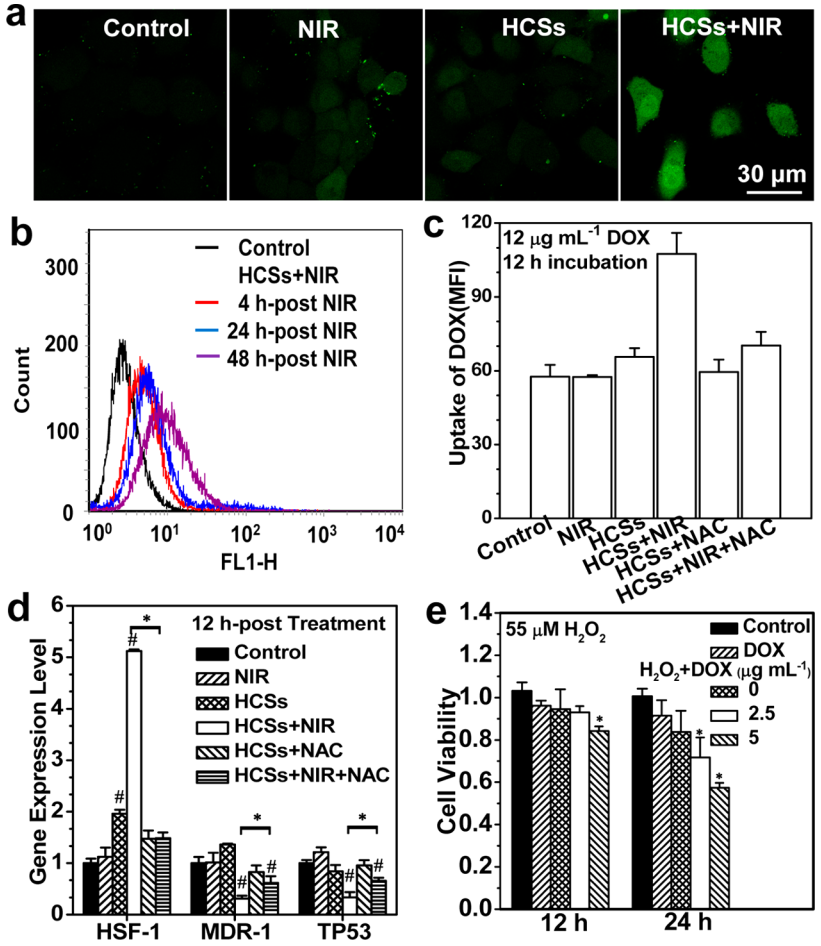

Figure 4. Overcoming DOX resistance by increasing redox status with irradiated HCSs. Changes in the cellular ROS level of MCF-7/ADR cells under irradiation according to (a) confocal images and (b) flow cytometry. Cells were exposed to 10 μg mL^{-1} HCSs beforehand and then irradiated by a 2.4 W cm^{-2} laser for 8 min. (c) According to flow cytometry, changes in accumulated DOX when laser-irradiated MCF-7/ADR cells were treated with/without the free radical inhibitor *N*-acetyl-cysteine (NAC). (d) Impact of intracellular ROS levels on the expression of HSF-1, MDR-1, and TP53 genes. The asterisk (*) shows significant differences between test samples and the sample under laser irradiation (HCSs + NIR) ($p < 0.05$); the pound symbol (#) indicates significant differences between test samples and the control. (e) Change in the DOX sensitivity of MCF-7/ADR cells treated with 55 μM H_2O_2. Asterisk (*) indicates significant differences between control and test samples. All data were described as mean value and standard derivation ($n = 3$).

nm femtosecond laser, a rapid photothermal conversion occurred in MCF-7/ADR cells after the uptake of HCSs for 24 h (Supporting Information Figure S2d). When we used a laser of a medium power density (2.4 W cm^{-2}), the irradiated cell pellet temperature reached 45 °C, which was not sufficient to cause acute cell death (10% death ratio). However, heat from a higher power-density laser-induced small blisters and ruptured the cell membranes to result in direct cell death.[53] As shown by TEM images, most HCSs remained in the endo/lysosomes or large vesicles after being internalized (Figure 2c, Supporting Information Figure S4a,b). However, after laser irradiation, some HCSs did enter the cytoplasm (Figure 2d, Supporting Information Figure S4c,d), which suggested that photothermal treatment could change the lysosomal membrane integrity and allow DOX to reach the cytoplasm. The integrity of the lysosomal membranes during laser irradiation was revealed by AO staining as shown in Figure 2e. Results from staining show that laser irradiation increased the lysosomal membrane permeation (LMP), while a separate treatment by laser irradiation or HCSs did not change the LMP because a fast temperature rise generated vapor cavitation that ruptured the membrane structure.[53,54] An increase in LMP may help the leakage of DOX@HCSs from lysosomes and allow for easier DOX entry to the nuclei.

DOX@HCSs were able to gradually release DOX in an acidic environment like the lysosomes, as shown by the DOX release profile in artificial lysosomal fluid (Supporting Information Figure S2f). There was limited DOX diffusion into the nucleus and therefore limited cell death. After irradiating of the cells, DOX@HCSs released DOX more quickly than nonirradiated states did and some of the DOX were able to target the nuclei after only 3 h, suggesting that the photothermal effects may combat DOX resistance (Supporting Information Figure S6). One reason was that DOX release depended on both temperature and pH. Under laser irradiation, the drug release rate became much faster because the laser-converted heat dissociated the strong interactions between DOX and the carbon matrix. We observed that an acidic environment of pH 4.5 produced a greater effect on DOX release in the nanospheres compared to a pH 7.0 environment (Supporting Information Figure S2e,f). Overall, results suggested that photothermal effects may accelerate the release of DOX from DOX@HCSs in the lysosomes and then enable the DOX to enter the nuclei (Figure 2f).

DOI: 10.1021/ja511560b
J. Am. Chem. Soc. 2015, 137, 1947−1955

Combatting Resistance under Laser Irradiation. After a 24 h uptake of HCSs or DOX@HCSs, MCF-7/ADR cells were irradiated with a 2.4 W cm^{-2} NIR laser for 8 min. Cell viability decreased, while laser irradiation alone caused negligible effects on viability. In contrast, DOX@HCSs caused a time-dependent cytotoxicity (Figure 3a) due to greater DOX accumulation (Figure 2a) and increased DOX release during irradiation (Figure 2f). Laser irradiation thus reduced the IC_{50} to 2.5 μg mL^{-1} 48 h post-NIR irradiation as shown by cell viability result in Figure 3b and improved the ability of cells to accumulate DOX (Figure 3c).

As reported previously,[55,56] the increased expression of the HSF-1 gene and the formation of hsf-1 protein homotrimers is known to suppress the expression of both Pgp protein and the mutant p53, which allows more DOX to accumulate inside cells and improves sensitivity to DOX. Therefore, the reduction in DOX resistance is highly dependent on the activation of the HSF-1 gene. The effects of laser irradiation on the resistance of MCF-7/ADR and possible mechanisms are illustrated in Supporting Information Figure S8. As shown in Supporting Information Figure S8c, a minimal DOX was observed entering the nuclei when MCF-7/ADR cells were treated with HCSs and DOX together. In contrast, 48 h after irradiation, high amount of DOX was distributed inside the nuclei for these cells. These results indicated that laser irradiation resulted in greater DOX accumulation inside the nucleus most likely via an HSF-1 gene-mediated pathway after photothermal stimulus.[17] Meanwhile, the expression of resistance-related molecules, such as HSF-1 gene or its encoding hsf-1 protein, TP53 or the mutated p53, and MDR-1 or its encoding Pgp was modulated to decrease the resistance of MCF-7/ADR cells toward DOX (Figure 3d–f).

We next used quercetin (QUT), an HSF-1 gene inhibitor[57] that suppresses the expression of the HSF-1 gene, to treat MCF-7/ADR cells. After irradiation alone, the intracellular mRNA levels of HSF-1 were maintained at a low level (Figure 3d), which allowed MCF-7/ADR cells to remain resistant with high levels of mutant p53 and Pgp (Figure 3e). However, laser irradiation stimulated the expression of the HSF-1 gene and the formation of homotrimers of hsf-1 protein that can translocate to the nuclei, thereby suppressing the resistance pathway (Figure 3f). When laser irradiation and DOX treatment were combined, cell viability decreased to ca. 50% at 48 h. But when QUT was added, cell viability remained at approximately 70%, similar to behavior observed under laser irradiation alone (Supporting Information Figure S7b). Laser irradiation did appear to activate HSF-1 gene expression and thereby will help combat DOX resistance.

HCSs as ROS Generators To Persistently Combat Chemoresistance. After laser irradiation, MCF-7/ADR cells containing HCSs remained in a DOX-sensitive state for 48 h (Figure 3b). This relatively long period suggested that other factors might be playing a more prominent role than anticipated in combatting resistance. We observed that the free radical levels in MCF-7/ADR cells were significantly lower compared to that in the DOX-sensitive cells (Supporting Information Figure S8a,b), indicating that a distinct redox state likely contributed to DOX resistance. The selective pressure of toxic therapeutic agents favors the evolution of cancer cells with mutated genes that support drug resistance including more powerful cellular systems for scavenging free radicals. The resistant cells can thus maintain a low redox status, retain normal metabolic functions, and are more resistant to cell death following exposure to chemotherapeutic drugs.[7,9] Disturbance of the redox state in resistant cells seems to be an attractive choice for combatting resistance.

To explore this avenue, we used NIR laser irradiation on the internalized HCSs to increase the redox state. After laser irradiation, MCF-7/ADR cells retained a higher ROS level than the control or HCSs, DOX@HCSs, or laser irradiation-treated cells (Figure 4a). The increased production of intracellular free radicals was time-dependent (Figure 4b, Supporting Information Figure S8d,e). Light-activated free radical production depended on time and reached a maximum after 48 h (Supporting Information Figure S8e), which helped sensitize MCF-7/ADR cells to DOX via greater accumulation (Figure 3c), and caused translocation of DOX to the nucleus (Supporting Information Figures S7a and 8c).

To elucidate the major role of ROS in overcoming resistance, the ROS inhibitor *N*-acetyl-cysteine (NAC) was used to illustrate how the redox state changes the nature of the resistance. Laser irradiation increased the production of cellular ROS. After treatment with NAC, MCF-7/ADR cells maintained a lower ROS level (Supporting Information Figure S8e) and also remained in a resistant state, as shown by the activity of resistance-related genes and DOX accumulation (Figure 4c,d). NAC efficiently inhibited changes in the mRNA levels of HSF-1, MDR-1, and TP53 genes that were induced by an irradiation stimulus. Moreover, an elevated ROS level produced by adding H_2O_2 significantly increased the sensitivity of MCF-7/ADR cells to DOX (Figure 4e). This meant that the increased redox state caused by laser irradiation may be responsible for increased sensitivity of cells to DOX.

To identify the types of free radicals, we used electron spin resonance (ESR) to study the electron structure and properties of HCSs in the presence and absence of NIR irradiation. On the basis of ESR signal intensity and its double integration area, HCSs had free electrons which can induce free radicals with a 2.0026 G factor; the signal was significantly increased under several minutes of NIR irradiation (Figure 5a, Supporting Information Figure S9a,b). NIR irradiation for 8 min increased the production of free radicals which reached equilibrium at 15 min (Supporting Information Figure S9b). Following irradiation, the production of free radicals largely depended on the concentration of HCSs and time post-NIR irradiation.

The accumulation of free radicals was monitored by measuring CP nitroxide (CP·) due to the oxidation of 1-hydroxy-3-carboxy-2,2,5,5- tetramethylpyrrolidine (CPH). CPH can be oxidized to CP· radicals, giving a typical ESR spectrum of three lines with intensity ratios of 1:1:1. NIR irradiation increased the amount of CP· radicals oxidized by HCSs in a time- and dose-dependent manner (Figure 5b, Supporting Information Figure S9c). HCSs can induce higher level of free radicals under longer irradiation. After irradiation, the oxidation of CPH to CP· increased with incubation/reaction time, suggesting that laser irradiation increased the catalytic properties of the HCSs.

To explore this further, we studied the species of free radicals induced by HCSs and NIR irradiation. The spin trap 5-(diethoxyphosphoryl)-5-methyl-1-pyrroline-*N*-oxide (DEPMPO) was used to study free electrons in the systems. After DEPMPO and H_2O_2 were added to HCSs, the ESR spectra of DEPMPO/·OH adducts showed that both HCSs and NIR irradiation catalyzed the production of ·OH radicals (Figure 5c). When Epigallocatechin gallate (EGCG) was added to interact with ·OH and scavenge it from the systems, no

DOI: 10.1021/ja511560b
J. Am. Chem. Soc. 2015, 137, 1947–1955

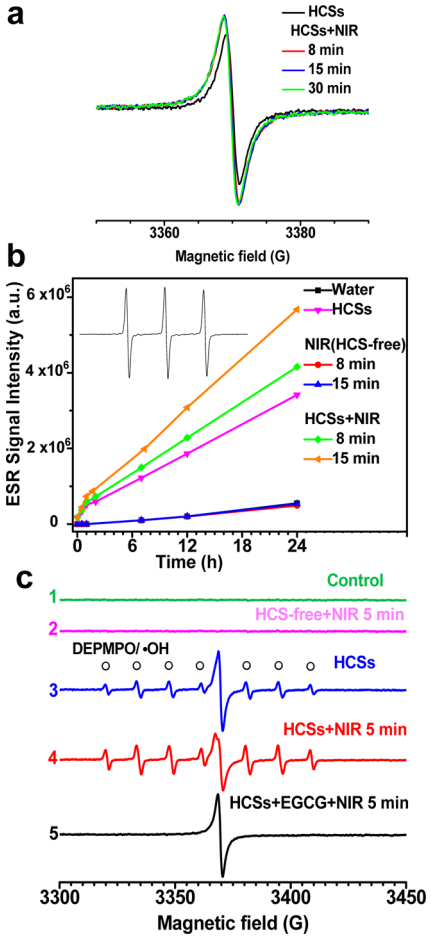

Figure 5. Production of free radicals by HCSs under NIR laser irradiation. (a) ESR spectra of 4.5 mg mL^{-1} HCSs and those under a 5 W power NIR laser irradiation for 8, 15, and 30 min. (b) Time-dependent accumulation of free radicals based on the oxidation of HCSs on CPH. ESR signal intensity of CP· with time in the absence and presence of 40 μg mL^{-1} HCSs: without irradiation, with laser irradiation for 8 min, and with laser irradiation for 15 min. (c) ESR spectra of DEPMPO/·OH adducts in the present of 20 mM DEPMPO and 5 mM H_2O_2. (1) control, (2) control with laser irradiation for 5 min, (3) 200 μg mL^{-1} HCSs, (4) HCSs with laser irradiation for 5 min, and (5) adding 2 mM EGCG in HCSs with laser irradiation for 5 min. The open circle symbol (○) indicates the lines of the characteristic ESR signal for DEPMPO/·OH. All the spectra are recorded and averaged from 9 scans.

DEPMPO/·OH adduct was formed, but the single line spectrum of the HCSs themselves also exhibited a unique signalwas still present (Figure 5c). HCSs also catalyzed the transient production of singlet oxygen ($^1O_2$) during NIR irradiation. We identified the $^1O_2$ based on the emission spectra of the $^1O_2$ fluorescene probe 1,3-Diphenylisobenzofuran (DPBF) (Supporting Information Figure S10a–d). After NIR irradiation of the HCSs, $^1O_2$ was immediately generated with the amount depending on the irradiation time (Supporting Information Figure S10e,f). The HCSs were able to catalyze both $^1O_2$ and ·OH production and induce increased production of ·OH radicals as a result of changes in their electron transport properties under laser irradiation. HCSs alone induced a 80% rise in the cellular ROS level, while HCSs with laser irradiation resulted in a 250% increase of cellular ROS levels 48 h postirradiation (Supporting Information Figure S8e) in agreement with our ESR experiments (Figure 5b,c).

To the best of our knowledge, three factors account for the light-induced free radical generation. First, the surface structures of carbon play an important role. As shown by Raman spectra (Figure 1g), HCSs have both sp^2- and sp^3-hybridized carbon atoms and the structural characteristics of graphene endow them with unique electronic and chemical properties that catalyze the oxidation of small molecules even under relatively mild conditions.[58−60] The dangling electrons in sp^2 and sp^3 carbon atoms make these carbon nanomaterials chemically active, allowing them to catalyze oxidation and produce ROS such as hydrogen peroxide or hydroxyl radicals[48,49] while also promoting H_2O_2 to form ·OH in biological systems.[44] Some stress states such as a temperature increase and H_2O_2 can trigger ·OH formation due to an interplay between the components of the electron transfer chain and sp^2, sp^3 carbon structures.[44,61] Second, laser irradiation changes the characteristics of HCSs and the local environment within the cells. Exposure of HCSs to short pulse laser irradiation not only produces shock photoacoustic waves,[59,62] but also activates carbon-steam chemical reactions on carbon nanoparticles at high temperature and pressure due to rapid heating and cooling.[63,64] NIR irradiation on the HCSs also induced the generation of singlet oxygen ($^1O_2$) and these free radicals may improve the HCS catalytic performance. Laser irradiation probably produced a more active surface on HCSs that in turn influenced electron transport and increased their capacity to accept or donate electrons in the cytoplasm or mitochondria. Third, results demonstrate that laser irradiation of HCSs can produce photoacoustic forces and vaporization that rupture the lysosomal membranes and release HCSs into the cytoplasm. The sp^2 and sp^3 carbon atoms on HCSs thus more easily catalyzed the conversion of small molecules in the cytoplasm to stronger free radicals and trigger persistent ROS.

The particle size and dispersion properties of nanoparticles are critical to their use in biomedical applications. Generally, carbon nanoparticles are prepared at high temperatures. Due to the high surface energy of these nanoparticles and high temperature sintering effects, these particles are barely redispersed in solution. This difficulty becomes even greater as these carbon particles become smaller, for example, below 100 nm. Our synthesis produced solvent-dispersible, discrete, uniform, and biocompatible HCSs that can be used as drug carriers in the biomedical fields. The mesopore channels and hollow void of the HCSs provide excellent drug loading capacity as compared with other carbonaceous nanocarriers.[31,65] For biomedical applications, our HCSs exhibit better dispersion in aqueous solutions than other carbonaceous nanomaterials, which usually require the use of polyethylene glycol, surfactants, and macromolecules for good dispersion.[28−30]

Adding to their utility, these HCSs have strong photothermal transition abilities and can promote the generation of free radicals under laser irradiation. Use of ROS in combination with hyperthermia has been reported to sensitize chemotherapy,[66] but a multifunctional platform that realizes both modes simultaneously is highly desired for nanomedicine. The present study has shown that laser-irradiated HCSs can efficiently sensitize resistant cells to DOX by simultaneously realizing thermal effects and increasing the redox state in a time-dependent manner. For HCSs, the initial activation of the HSF-1 gene expression is due to photothermal stimuli, and its

DOI: 10.1021/ja511560b
J. Am. Chem. Soc. 2015, 137, 1947−1955

continuation is induced by the persistent generation of ROS. Then, the formation of the hsf-1 protein homotrimer facilitates the combatting of resistance for a long time. Given these advantages, the HCSs should be considered as an excellent platform for combatting chemoresistance in conjunction with synergistic chemotherapy and laser irradiation stimuli to produce heat and free radicals.

CONCLUSIONS

We have designed and tested a novel platform, HCSs, for combatting chemoresistance using synergistic chemical therapy and laser irradiation stimuli to produce heat and free radicals (Figure 6). These HCSs have a high load capacity, and can deliver a large amount of a drug into cells. Moreover, laser irradiation of HCSs can not only induce photothermal effects but also disrupt the cellular redox state, which releases persistent free radicals that enhance HSF-1 gene expression and promote the production of hsf-1 protein homotrimers to suppress resistance-related pathways. The viability of resistant cells is reduced because laser excitation of DOX@HCSs not only releases DOX but also serves as a ROS generator by triggering the generation of more free radicals. On the basis of these means of suppressing resistance, the sp^2 and sp^3 carbon-based DOX@HCS formulation holds promise in cancer therapy and should also be explored further as a means to prevent chemoresistance.

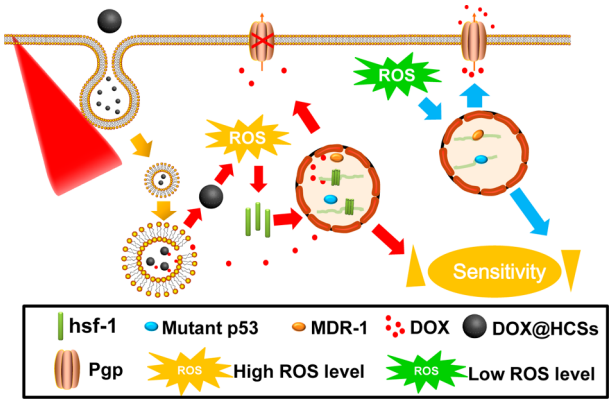

Figure 6. Combatting the chemotherapeutic resistance of cancer using hollow carbon nanospheres under NIR laser irradiation. Resistant cancer cells usually maintain a low redox state to survive in the presence of toxic DOX. MDR-1 regulates Pgp expression in charge of DOX efflux, while mutant TP53 encodes mutant p53 protein that decreases cell sensitivity to drugs. Laser irradiation can not only produce photothermal effects to promote DOX release and transfer from lysosomal DOX@HCSs to nuclei, but also activate the HCS surface to generate persistent free radicals. The increased levels of free radicals play a crucial role in combatting drug resistance by driving the formation of hsf-1 protein homotrimers. These homotrimers finally suppress the expression of the MDR-1 and mutant TP53 genes which enable the resistance.

ASSOCIATED CONTENT

Supporting Information

Online figures about experimental methods and results. These methods include the synthesis and characterization of HCSs, the loading and release of DOX, the cell viability assay, laser irradiation, ESR measurements, cellular uptake and localization of DOX and DOX@HCSs, changes in the integrity of lysosomal membranes, the cellular ROS levels, and the gene and protein expression of MCF-7/ADR cells after irradiation. These results include a scheme of the process to load DOX inside HCSs, the characterization of DOX@HCSs, the cytotoxicity of DOX, HCSs, and DOX@HCSs to the cells, TEM images for cells containing HCSs with/without irradiation, the generation of singlet oxygen and hydroxyl radicals under laser irradiation, the impact of irradiation on the cell viability, the cell death ratio, DOX release, and ROS levels for DOX@HCS or HCS-contained cells. This material is available free of charge *via* the Internet at http://pubs.acs.org.

AUTHOR INFORMATION

Corresponding Authors

chenchy@nanoctr.cn
anhuilu@dlut.edu.cn

Author Contributions

‖These authors contributed equally.

Notes

The authors declare no competing financial interest.

ACKNOWLEDGMENTS

We are grateful for financial support by the National Basic Research Program of China (2012CB934000 and 2011CB933401), the National Natural Science Foundation of China (11205166, 21225312, and 21320102003), the National Science Fund for Distinguished Young Scholars (No.11425520), the International Science & Technology Cooperation Program of China (2013DFG32340), the Major Equipment Program (2011YQ030134) from the Ministry of Science Technology of China, and the German Federal Ministry of Education and Research (BMBF 0315773A). The work was also partially supported by a regulatory science grant under the FDA Nanotechnology CORES Program (JY). We appreciate Prof. Meihua Sui of Zhejiang University for discussion on cell culture experiment, Miss Jing Liu at NCNST for $^1O_2$ measurement, and Dr. Ru Liu at IHEP for assistance with confocal imaging. We are grateful to Dr. Ann Motten from NIEHS/NIH and Prof. Peter Thrower for their comments on the manuscript. We thank Dr. Lili Fox Vélez for her scientific editing.

REFERENCES

(1) Gottesman, M. M. *Annu.Rev. Med.* **2002**, *53*, 615−627.
(2) Buzdar, A. U.; Marcus, C.; Smith, T. L.; Blumenschein, G. R. *Cancer* **1985**, *55*, 2761−2765.
(3) Wong, E.; Giandomenico, C. M. *Chem. Rev.* **1999**, *99*, 2451−2466.
(4) Gottesman, M. M.; Fojo, T.; Bates, S. E. *Nat. Rev. Cancer* **2002**, *2*, 48−58.
(5) Brown, J. M.; Wouters, B. G. *Cancer Res.* **1999**, *59*, 1391−1399.
(6) Aas, T.; Borresen, A. L.; Geisler, S.; Smith-Sorensen, B.; Johnsen, H.; Varhaug, J. E.; Akslen, L. A.; Lonning, P. E. *Nat. Med.* **1996**, *2*, 811−814.
(7) Åkerfelt, M.; Morimoto, R. I.; Sistonen, L. *Nat. Rev. Mol. Cell Biol.* **2010**, *11*, 545−555.
(8) Trachootham, D.; Alexandre, J.; Huang, P. *Nat. Rev. Drug Discovery* **2009**, *8*, 579−591.
(9) Pelicano, H.; Carney, D.; Huang, P. *Drug Resist. Update* **2004**, *7*, 97−110.
(10) Wang, F.; Wang, Y. C.; Dou, S.; Xiong, M. H.; Sun, T. M.; Wang, J. *ACS Nano* **2011**, *5*, 3679−3692.
(11) Gao, Y.; Chen, Y.; Ji, X. F.; He, X. Y.; Yin, Q.; Zhang, Z. W.; Shi, J. L.; Li, Y. P. *ACS Nano* **2011**, *5*, 9788−9798.

DOI: 10.1021/ja511560b
J. Am. Chem. Soc. 2015, 137, 1947−1955

(12) Liang, X. J.; Meng, H.; Wang, Y. Z.; He, H. Y.; Meng, J.; Lu, J.; Wang, P. C.; Zhao, Y. L.; Gao, X. Y.; Sun, B. Y.; Chen, C. Y.; Xing, G. M.; Shen, D. W.; Gottesman, M. M.; Wu, Y.; Yin, J. J.; Jia, L. *Proc. Natl. Acad. Sci. U.S.A.* **2010**, *107*, 7449−7454.
(13) Wang, F. H.; Zhang, D. R.; Zhang, Q.; Chen, Y. X.; Zheng, D. D.; Hao, L. L.; Duan, C. X.; Jia, L. J.; Liu, G. P.; Liu, Y. *Biomaterials* **2011**, *32*, 9444−9456.
(14) Meng, H.; Mai, W. X.; Zhang, H. Y.; Xue, M.; Xia, T.; Lin, S. J.; Wang, X.; Zhao, Y.; Ji, Z. X.; Zink, J. I.; Nel, A. E. *ACS Nano* **2013**, *7*, 994−1005.
(15) Meng, H.; Liong, M.; Xia, T.; Li, Z. X.; Ji, Z. X.; Zink, J. I.; Nel, A. E. *ACS Nano* **2010**, *4*, 4539−4550.
(16) Szakács, G.; Paterson, J. K.; Ludwig, J. A.; Booth-Genthe, C.; Gottesman, M. M. *Nat. Rev. Drug Discovery* **2006**, *5*, 219−234.
(17) Wang, L. M.; Lin, X. Y.; Wang, J.; Hu, Z. J.; Ji, Y. L.; Hou, S.; Zhao, Y. L.; Wu, X. C.; Chen, C. Y. *Adv. Funct. Mater.* **2014**, *24*, 4229−4239.
(18) Yu, H. J.; Xu, Z. A.; Chen, X. Z.; Xu, L. L.; Yin, Q.; Zhang, Z. W.; Li, Y. P. *Macromol. Biosci.* **2014**, *14*, 100−109.
(19) Chen, J. L.; Solomides, C.; Simpkins, H. *Biochem. Biophys. Res. Commun.* **2014**, *447*, 77−82.
(20) Min, Y. Z.; Mao, C. Q.; Chen, S. M.; Ma, G. L.; Wang, J.; Liu, Y. Z. *Angew. Chem., Int. Ed.* **2012**, *51*, 6742−6747.
(21) Tay, C. Y.; Setyawati, M. I.; Xie, J. P.; Parak, W. J.; Leong, D. T. *Adv. Funct. Mater.* **2014**, *24*, 5936−5955.
(22) Zhang, Z. J.; Wang, L. M.; Wang, J.; Jiang, X. M.; Li, X. H.; Hu, Z. J.; Ji, Y. L.; Wu, X. C.; Chen, C. Y. *Adv. Mater.* **2012**, *24*, 1418−1423.
(23) Yamakoshi, Y.; Umezawa, N.; Ryu, A.; Arakane, K.; Miyata, N.; Goda, Y.; Masumizu, T.; Nagano, T. *J. Am. Chem. Soc.* **2003**, *125*, 12803−12809.
(24) Minai, L.; Yeheskely-Hayon, D.; Yelin, D. *Sci. Rep.* **2013**, *3*, 2146.
(25) Pasparakis, G. *Small* **2013**, *9*, 4130−4134.
(26) Yin, J. J.; Liu, J.; Ehrenshaft, M.; Roberts, J. E.; Fu, P. P.; Mason, R. P.; Zhao, B. Z. *Toxicol. Appl. Pharmacol.* **2012**, *263*, 81−88.
(27) Xu, L. G.; Liu, Y.; Chen, Z. Y.; Li, W.; Liu, Y.; Wang, L. M.; Liu, Y.; Wu, X. C.; Ji, Y. L.; Zhao, Y. L.; Ma, L. Y.; Shao, Y. M.; Chen, C. Y. *Nano Lett.* **2012**, *12*, 2003−2012.
(28) Liu, Z.; Robinson, J. T.; Sun, X. M.; Dai, H. J. *J. Am. Chem. Soc.* **2008**, *130*, 10876−10877.
(29) Zhang, L. M.; Xia, J. G.; Zhao, Q. H.; Liu, L. W.; Zhang, Z. J. *Small* **2010**, *6*, 537−544.
(30) Liu, Z.; Fan, A. C.; Rakhra, K.; Sherlock, S.; Goodwin, A.; Chen, X. Y.; Yang, Q. W.; Felsher, D. W.; Dai, H. J. *Angew. Chem., Int. Ed.* **2009**, *48*, 7668−7672.
(31) Chen, Y.; Xu, P. F.; Shu, Z.; Wu, M. Y.; Wang, L. Z.; Zhang, S. J.; Zheng, Y. Y.; Chen, H. R.; Wang, J.; Li, Y. P.; Shi, J. L. *Adv. Funct. Mater.* **2014**, *24*, 4386−4396.
(32) Fang, Y.; Gu, D.; Zou, Y.; Wu, Z. X.; Li, F. Y.; Che, R. C.; Deng, Y. H.; Tu, B.; Zhao, D. Y. *Angew. Chem., Int. Ed.* **2010**, *49*, 7987−7991.
(33) Lu, A. H.; Sun, T.; Li, W. C.; Sun, Q.; Han, F.; Liu, D. H.; Guo, Y. *Angew. Chem., Int. Ed.* **2011**, *50*, 11765−11768.
(34) Wang, G. H.; Sun, Q.; Zhang, R.; Li, W. C.; Zhang, X. Q.; Lu, A. H. *Chem. Mater.* **2011**, *23*, 4537−4542.
(35) Wang, S.; Li, W. C.; Hao, G. P.; Hao, Y.; Sun, Q.; Zhang, X. Q.; Lu, A. H. *J. Am. Chem. Soc.* **2011**, *133*, 15304−15307.
(36) Sun, Q.; Li, W. C.; Lu, A. H. *Small* **2013**, *9*, 2086−2090.
(37) Liu, J.; Qiao, S. Z.; Liu, H.; Chen, J.; Orpe, A.; Zhao, D. Y.; Lu, G. Q. *Angew. Chem., Int. Ed.* **2011**, *50*, 5947−5951.
(38) Ganeshkumar, M.; Ponrasu, T.; Sathishkumar, M.; Suguna, L. *Colloids Surf., B* **2013**, *103*, 238−243.
(39) Fang, Y.; Zheng, G. F.; Yang, J. P.; Tang, H. S.; Zhang, Y. F.; Kong, B.; Lv, Y. Y.; Xu, C. J.; Asiri, A. M.; Zi, J.; Zhang, F.; Zhao, D. Y. *Angew. Chem., Int. Ed.* **2014**, *53*, 5366−5370.
(40) Zhu, J.; Liao, L.; Bian, X. J.; Kong, J. L.; Yang, P. Y.; Liu, B. H. *Small* **2012**, *8*, 2715−2720.
(41) Ge, C. C.; Du, J. F.; Zhao, L.; Wang, L. M.; Liu, Y.; Li, D. H.; Yang, Y. L.; Zhou, R. H.; Zhao, Y. L.; Chai, Z. F.; Chen, C. Y. *Proc. Natl. Acad. Sci. U.S.A.* **2011**, *108*, 16968−16973.
(42) Hu, W. B.; Peng, C.; Lv, M.; Li, X. M.; Zhang, Y.; Chen, N.; Fan, C. H.; Huang, Q. *ACS Nano* **2011**, *5*, 3693−3700.
(43) Su, D. S.; Perathoner, S.; Centi, G. *Chem. Rev.* **2013**, *113*, 5782−5816.
(44) Zhang, W. D.; Wang, C.; Li, Z. J.; Lu, Z. Z.; Li, Y. Y.; Yin, J. J.; Zhou, Y. T.; Gao, X. F.; Fang, Y.; Nie, G. J.; Zhao, Y. L. *Adv. Mater.* **2012**, *24*, 5391−5397.
(45) Li, Y.; Liu, Y.; Fu, Y. J.; Wei, T. T.; Guyader, L. L.; Gao, G.; Liu, R. S.; Chang, Y. Z.; Chen, C. Y. *Biomaterials* **2011**, *33*, 402−411.
(46) Manna, S. K.; Sarkar, S.; Barr, J.; Wise, K.; Barrera, E. V.; Jejelowo, O.; Rice-Ficht, A. C.; Ramesh, G. T. *Nano Lett.* **2005**, *5*, 1676−1684.
(47) Shvedova, A.; Castranova, V.; Kisin, E.; Schwegler-Berry, D.; Murray, A.; Gandelsman, V.; Maynard, A.; Baron, P. *J. Toxicol. Environ. Health, PartA* **2003**, *66*, 1909−1926.
(48) Chen, R. Z.; Pignatello, J. J. *Environ. Sci. Technol.* **1997**, *31*, 2399−2406.
(49) Xu, W. Q.; Dana, K. E.; Mitch, W. A. *Environ. Sci. Technol.* **2010**, *44*, 6409−6415.
(50) Wu, S. L.; Zhao, X. D.; Li, Y. H.; Du, Q. J.; Sun, J. K.; Wang, Y. H.; Wang, X.; Xia, Y. Z.; Wang, Z. H.; Xia, L. H. *Materials* **2013**, *6*, 2026−2042.
(51) Duffy, P.; Magno, L. M.; Yadav, R. B.; Roberts, S. K.; Ward, A. D.; Botchway, S. W.; Colavita, P. E.; Quinn, S. J. *J. Mater. Chem.* **2012**, *22*, 432−439.
(52) Ferrari, A. C.; Meyer, J. C.; Scardaci, V.; Casiraghi, C.; Lazzeri, M.; Mauri, F.; Piscanec, S.; Jiang, D.; Novoselov, K. S.; Roth, S.; Geim, A. K. *Phys. Rev. Lett.* **2006**, *97*, 187401.
(53) Tong, L.; Zhao, Y.; Huff, T. B.; Hansen, M. N.; Wei, A.; Cheng, J. X. *Adv. Mater.* **2007**, *19*, 3136−3141.
(54) Lukianova-Hleb, E. Y.; Ren, X. Y.; Zasadzinski, J. A.; Wu, X. W.; Lapotko, D. O. *Adv. Mater.* **2012**, *24*, 3831−3837.
(55) Kanagasabai, R.; Krishnamurthy, K.; Druhan, L. J.; Ilangovan, G. *J. Biol. Chem.* **2011**, *286*, 33289−33300.
(56) Krishnamurthy, K.; Vedam, K.; Kanagasabai, R.; Druhan, L. J.; Ilangovan, G. *Proc. Natl. Acad. Sci. U.S.A.* **2012**, *109*, 9023−9028.
(57) Singh, V.; Aballay, A. *Proc. Natl. Acad. Sci. U.S.A.* **2006**, *103*, 13092−13097.
(58) Liu, X.; Frank, B.; Zhang, W.; Cotter, T. P.; Schlögl, R.; Su, D. S. *Angew. Chem., Int. Ed.* **2011**, *50*, 3318−3322.
(59) Dreyer, D. R.; Jia, H. P.; Bielawski, C. W. *Angew. Chem., Int. Ed.* **2010**, *49*, 6813−6816.
(60) Frank, B.; Blume, R.; Rinaldi, A.; Trunschke, A.; Schlögl, R. *Angew. Chem., Int. Ed.* **2011**, *50*, 10226−10230.
(61) Zhou, H. J.; Zhang, B.; Zheng, J. J.; Yu, M. F.; Zhou, T.; Zhao, K.; Jia, Y. X.; Gao, X. F.; Chen, C. Y.; Wei, T. T. *Biomaterials* **2014**, *35*, 1597−1607.
(62) Chen, H. X.; Diebold, G. *Science* **1995**, *270*, 963−966.
(63) McGrath, T. E.; Diebold, G. J.; Bartels, D. M.; Crowell, R. A. *J. Phys. Chem. A* **2002**, *106*, 10072−10078.
(64) Chen, H. X.; McGrath, T.; Diebold, G. J. *Angew. Chem., Int. Ed.* **1997**, *36*, 163−166.
(65) Toh, T. B.; Lee, D. K.; Hou, W. X.; Abdullah, L. N.; Nguyen, J.; Ho, D.; Chow, E. K. H. *Mol. Pharmaceutics* **2014**, *11*, 2683−2691.
(66) Wang, C. C.; Chen, F.; Kim, E.; Harrison, L. E. *Surgery* **2007**, *142*, 384−392.

DOI: 10.1021/ja511560b
J. Am. Chem. Soc. 2015, 137, 1947−1955